

Received July 27, 2018, accepted August 29, 2018, date of publication September 3, 2018, date of current version December 7, 2018.

Digital Object Identifier 10.1109/ACCESS.2018.2868418

# Traffic Flow Detection Using Distributed Fiber Optic Acoustic Sensing

HUIYONG LIU<sup>1</sup>, JIHUI MA<sup>ID1</sup>, WENFA YAN<sup>1</sup>, WENSHENG LIU<sup>2</sup>,  
XI ZHANG<sup>1</sup>, AND CONGCONG LI<sup>1</sup>

<sup>1</sup>MOE Key Laboratory of Urban Transportation Complex System Theory and Technology,  
Beijing Jiaotong University, Beijing 100044, China

<sup>2</sup>Nanshan Mine, Magang (Group) Holding Co., Ltd., Ma'anshan 243061, China

Corresponding author: Jihui Ma (jhma@bjtu.edu.cn)

This work was supported by the National Natural Science Foundation of China under Grant 71621001.

**ABSTRACT** This paper proposes a novel method for traffic flow detection using distributed optical fiber acoustic sensing (DAS). Different from the traditional traffic flow detection method, this method detects the traffic vibration signal using a fiber optic cable. Distributed fiber-optic acoustic sensing technology can provide fully distributed acoustic information along the entire fiber link, and thus external acoustic signals from an arbitrary point can be detected and located. This paper uses DAS to obtain traffic vibration data. Using the characteristics of traffic vibration data, this paper proposes an improved wavelet threshold algorithm and an improved dual-threshold algorithm and verifies the feasibility and effectiveness of these methods. Finally, the experimental results from a vehicle-counting test show that the counting error is smaller for a single vehicle passing through the detection area and that the counting error is larger if multiple vehicles pass through the detection area continuously. In vehicle speed estimation, the results show good accuracy, and the error range is controlled to less than 6%.

**INDEX TERMS** Distributed optical fiber acoustic sensing (DAS), traffic flow, vehicle counting, vehicle speed estimation.

## I. INTRODUCTION

With the development of science and technology, intelligent traffic has attracted great attention in the field of traffic study, and intelligent monitoring of traffic flow in real time and supply of a command decision-making basis for traffic management have become urgent problems [1].

In traffic flow detection, accuracy and efficiency are essential for intelligent traffic management. With good detection, intelligent traffic management can adjust traffic signal control and traffic regulation, reduce traffic congestion, and detect abnormal behavioral events using timely response [2]. In intelligent traffic detection, the acquisition of traffic flow and other parameters is an indispensable component.

Currently, in the field of traffic flow detection, detection technology is divided into four main categories: video detection technology, magnetic detection technology, radar detection technology and wireless sensor network technology. Video-based traffic flow detection technology is a non-contact passive detection technology that tracks the behavior process of the traffic flow by analyzing continuous videos and images [3]. Magnetic-based traffic flow detection technology detects vehicle signals in the geomagnetic field using

ferromagnetic materials to change the properties of the surrounding magnetic field [4]. Radar-based traffic flow detection technology is the earliest method of vehicle speed detection, and the principle relies on transmission of radio waves through a certain frequency to detect a moving object. The object reflects the wave at different frequencies, which are used to calculate the speed of the moving object and detect the vehicle [5]. Traffic flow detection technology based on a wireless sensor network uses information collection nodes laid on the roadside to collect signals from the observation area, process the original signal and extract traffic information, and the information is transmitted through the wireless network [6].

However, existing methods such as video technology have high costs of installation and maintenance, and the detection effect is sensitive to environmental and weather conditions [7]. Magnetic technology is difficult to install and maintain and is easily damaged and influenced by the environment and other factors [8]. Radar detection technology is affected by the Doppler effect [9], and wireless sensor network technology is affected by the communication environment and the node performance [10]. In contrast, if distributed

acoustic sensing technology is used to explore traffic flow detection, i.e., use of distributed optical fiber acoustic sensing (DAS), the core components and corresponding programs and optical cables are used to achieve traffic detection, discrimination and counting [11]. Compared with traditional traffic flow detection, traffic flow detection based on distributed acoustic sensing technology is more sensitive and concealed and offers lower cost and higher resistance to temperature, corrosion, and electromagnetic interference. The most important feature is that the linkage of all data acquisition points can perceive an external signal to complete real-time blind spot detection of external signals.

Nima Riahi et al. used independent seismometers to detect moving objects with speeds of  $25 \pm 3$  m/s on roads, which may be vehicles running on the road. Because no actual traffic flow data are available for comparison, it is impossible to verify whether the moving source is a moving vehicle or not, but this approach offers the basic ideas and methods for monitoring of vehicle flow using seismic waves [12]. E Martin N Lindsey D Shan et al. deployed DAS equipment on a road north of Fairbanks, AK. According to waveform analysis, most of the noise on the road is due to vehicles. This work proved that it is feasible to use DAS to detect the traffic flow [13].

The main objective of this paper is to develop a more effective traffic flow detection method based on distributed acoustic sensing technology, which offers a new approach to solving the traffic flow detection problem. Certain experiments based on vehicle vibration data collected on a mine road are implemented to verify the effectiveness of this method.

In the rest of this paper, Section 2 describes the distributed acoustic sensing technology and analysis method. Sections 3 and 4 introduce the improved algorithms for traffic vibration data. Section 5 reports the experimental setup and results. Finally, Section 6 presents conclusions from this paper.

## II. METHODOLOGY

The main traffic parameters include vehicle flow, traffic density, occupancy, speed, headway, vehicle classification, queue length, etc. Traffic parameters are important links in traffic monitoring and traffic management. Using detection, analysis and control of traffic flow parameters, road traffic capacity can be improved, traffic accidents can be reduced, and the traffic flow distribution of the road network can be reasonably adjusted. The traffic flow detection process is divided into two components: data acquisition and data processing. In this paper, DAS technology is used in data acquisition, and wavelet threshold denoising and the dual-threshold method are used in data processing.

### A. PRINCIPLES AND SENSING MECHANISMS OF DISTRIBUTED OPTICAL FIBER ACOUSTIC SENSING

Distributed optical fiber sensing technology includes distributed sensing technology based on backscattering, distributed sensing technology based on polarized light time

domain reflection, distributed sensing technology based on optical interference technology, and quasi-distributed sensing technology based on fiber Prague grating. The distributed optical fiber sensing technology based on backscatter is detected using backscattering from the points along the optical fiber, and distributed optical fiber sensing can be realized using the relationship between the backscattered light and the measured quantity (such as temperature, stress, vibration, etc.). The DAS technology used in this paper is based on backward scattering. DAS uses an ordinary optical fiber as the sensing medium instead of a special optical fiber special treatment (write grating, etc.) [14]. DAS technology can be divided into two types based on the interference principle and backscatter detection technology. The former uses the M-Z, Sagnac and composite structures to obtain the relevant location information and external physical information via the positioning algorithm and demodulation algorithm. The latter uses changes in the polarization, intensity, frequency shift and phase of the backscattered light to measure the external physical quantity. The types of sensor technology include phase-sensitive optical time domain reflection ( $\Phi$ -OTDR), polarized light optical time domain reflection (P-OTDR), Brillouin optical time domain reflection (B-OTDR), Raman optical time domain reflection (R-OTDR), etc. Among these,  $\Phi$ -OTDR is often chosen due to the long distance and high spatial resolution of the distributed vibration or acoustic sensor, with obvious advantages for the measurement of traffic vibration data. Therefore, this paper selects  $\Phi$ -OTDR technology to collect the traffic vibration signal.

$\Phi$ -OTDR can detect and locate the disturbance signal by analyzing the optical power of the backscattered light in the optical fiber along the distribution curve of the time axis. OTDR uses a narrow-line-width pulse laser as a light source. The output results from the interference of the Rayleigh-scattered light reflected back in the optical pulse width. Therefore, the pulse width can be divided into two components. In fact, the interference light can be equal to the two components of the pulse light and the corresponding coherent Rayleigh backscattered light's coherence and self-correlation result. The optical signal received by the detector can be expressed as follows:

$$I_{\text{total}} = I_{RB} + I'_{RB} + 2\gamma(\tau_{RB} - \tau'_{RB})\sqrt{I_{RB}I'_{RB}} \cos(\phi_{RB} - \phi'_{RB}) \quad (1)$$

where  $I_{RB}$ ,  $I'_{RB}$ ,  $\tau_{RB}$ , and  $\tau'_{RB}$  are the intensity, phase and delay of the Rayleigh backscatter signal of the two-part pulsed light; and  $\gamma$  is the coherence function.

When the pressure generated from the vibration of the sound or object is applied to the sensing cable, the length and refractive index of the sensing cable change due to the elastic light effect, which causes the phase change of the transmitted light in the sensing cable, i.e., formula 1 in which  $(\phi_{RB} - \phi'_{RB})$  changes. Formula (1) shows that the phase change results in changes in the backscattered light intensity, which can be achieved by signal demodulation. In addition, by introducing

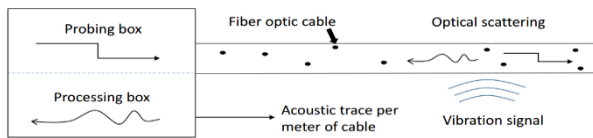


**FIGURE 1.** DAS working principle.

the OTDR, the vibration location can be accurately located, and the location of the disturbance can be obtained by measuring the time delay between the injected pulse and the received signal. The positioning accuracy  $\Delta z$  of the system is related to the pulse width  $T_p$  of the injected optical fiber and satisfies  $\Delta z = cT_p/2n$ , where  $c$  is the speed of light in a vacuum, and  $n$  is the refractive index of the transmission medium. A schematic of the principle of DAS is shown in Fig. 1.

### B. WAVELET THRESHOLD DE-NOISING

Wavelet denoising is an important application of wavelet analysis in the field of signal processing [15]. Three types of wavelets are addressed in denoising: wavelet denoising based on the wavelet transform modulus maximum principle, wavelet denoising based on wavelet coefficient correlation, and threshold wavelet denoising. Threshold denoising is a highly simple and effective wavelet denoising method proposed by D. L. Donoho. This algorithm can obtain the best estimation value in Besov space, but any other linear estimation cannot obtain the same estimation result.

#### 1) PRINCIPLE OF WAVELET THRESHOLD DENOISING

A signal model with noise can be described by the following:

$$f(t) = s(t) + \lambda e(t) \quad (t = 0, 1, \dots, n - 1) \quad (2)$$

where  $f(t)$  is a vibration signal with noise,  $e(t)$  is the noise,  $s(t)$  is the real signal, and  $\lambda$  is the noise level coefficient.

The study shows that the wavelet transform of the noisy signal is equal to the sum of the wavelet transform of the real signal and the wavelet transform of the noise. Using the wavelet transform, the energy of the real signal is concentrated in certain larger finite coefficients in the wavelet domain. However, the energy of the noise is distributed throughout the entire wavelet domain. Based on this principle, wavelet threshold denoising can decompose the signal with noise, keeping the low-frequency layer and addressing the noise in the high-frequency layer, and each layer goes through inverse coefficient reconstruction such that the processed signal is as close to the real signal as possible.

#### 2) STEP OF WAVELET THRESHOLD DENOISING

The main steps of the wavelet threshold denoising are described as follows:

(1) The signal with noise is transformed with the wavelet transform. Select a small wave basis and determine a hierarchical  $N$  for wavelet decomposition and subsequently perform  $N$ -layer wavelet decomposition for the signals.

(2) The wavelet coefficients of the high-frequency component are processed using threshold processing. Select an appropriate threshold, and the wavelet coefficient that is larger than the threshold can be considered using signal control and the wavelet coefficient that is less than the threshold that can be considered by noise control. The low-frequency wavelet coefficients are retained, and hard threshold denoising or soft threshold denoising is used to denoise the high-frequency coefficients of each layer of the first through  $N$  layers.

(3) The inverse transformation is used to reconstruct the real signal. The low-frequency coefficients obtained from the wavelet decomposition and the high-frequency coefficients of the first level to the  $N$  level after threshold denoising are reconstructed by the inverse wavelet transform, and the estimated values of the real signals are obtained.

### C. DUAL-THRESHOLD ALGORITHM

The dual-threshold algorithm performs detection using the product of short-term energy and short-term zero crossing rate. The basic goal is to determine the dual-threshold for the short-term energy and short-term zero crossing rate. One is a lower threshold, which is more sensitive to signal changes, and the other is a higher threshold, which is relatively less sensitive to signal changes. When the low threshold is exceeded, it might be caused by noise and is not necessarily the beginning of a vibration signal. When the high threshold is exceeded and the next time period is longer than the low threshold, this indicates the start of the vibration signal. The algorithm can detect the starting point and endpoint of the vibration signal using the characteristics of the zero crossing rate and energy.

#### 1) SHORT-TERM ENERGY

The energy of the signal is the main difference between the vibration signal and the noise, and the energy of the vibration signal is larger than that of the noise. The energy of the detected vibration signal is the sum of the energy of the noise segment and the vibration signal of the vehicle [16]. The traditional detection algorithm considers that if the environmental noise is sufficiently small to ensure the high signal-to-noise ratio of the system, the vehicle vibration signal can be separated from the noise background only by calculating the short-term energy of the input signal.

The short-term energy is defined as shown:

$$E_n = \sum_{m=-\infty}^{+\infty} [x(m)w(n-m)]^2 \quad (3)$$

where  $x(m)$  is a vibration signal,  $n$  is the sampling point,  $w(n)$  is the window function of movable finite length, and  $E_n$  is the short-term energy of the vibration signal at the  $N$  moment of the vibration signal.

The energy in the traffic vibration signal is more obvious than the change in time, and the energy of the general noise portion is much smaller than that of the vibration signal portion. The choice of window function plays a decisive role

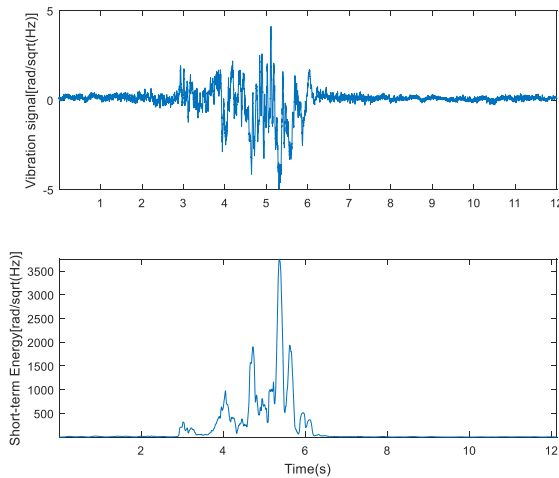


**FIGURE 2.** Typical traffic vibration signal and its short-term energy.

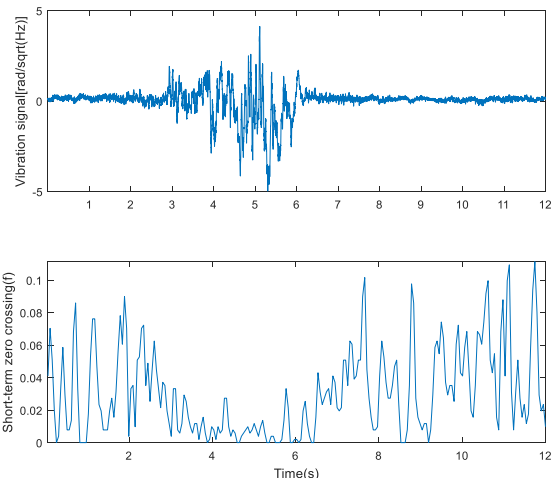
in the characteristics of the short-term energy representation. Short-term energy is used in the following aspects of the application. First, the short-term energy can be used to distinguish between the effective vibration signal and noise because the energy of the effective vibration signal is much larger than the energy of the noise. Second, the short-term energy can be used to determine the effective vibration signal and the invalid vibration signal. When identifying vibration signals, the short-term energy is usually used as a one-dimensional parameter in the feature that represents the magnitude of the vibration signal energy and the effective vibration signal information. For traffic vibration signal processing, the vibration signal is used first to eliminate the effect of zero mean drift (the value of the signal is subtracted from the average value of the original signal), and the resulting signal is subjected to short-term energy analysis. The vibration signal and short-term energy of the vibration signal are shown in Fig. 2.

Fig. 2 shows the effect of eliminating the bad points by controlling the width of the short-term energy, i.e., the signal is only required when the short-term energy of the signal continues to be greater than a certain value for a certain time.

In practice, it is difficult to guarantee such a high signal-to-noise ratio. Therefore, it is difficult to detect vehicle passage via the short-term energy.

## 2) SHORT-TERM ZERO CROSSING RATE

The short-term zero crossing rate is one of the simplest features in the time domain analysis of vibration signals and refers to the number of signals passing through zero values [2]. In the continuous vibration signal, the time domain waveform can be observed on the time axis. In the discrete vibration signal, the short-term zero crossing rate is essentially the number of symbol changes in the signal sampling points. The short-term zero crossing rate is the number of symbol changes, which can be regarded as a simple measure of the frequency of the signal. The short-term zero crossing rate can be used in the analysis of vibration signals.



**FIGURE 3.** Typical traffic vibration signal and its short-term zero crossing.

The short-term zero crossing rate is defined as follows:

$$Z_n = 1/2 \sum_{m=0}^{N-1} |sgn[x(m)] - sgn[x(m-1)]| \quad (4)$$

where  $sgn[]$  is a symbolic function, i.e.,

$$sgn[x] = \begin{cases} -1, & x < 0 \\ 1, & x \geq 0 \end{cases}$$

and  $x(m)$  is the vibration signal variable, and  $N$  is the window length.

The short-term zero crossing rate is a simple and effective method for analyzing the vibration signal. The short-term zero crossing rate is analyzed for the original signal, and the results are shown in Fig. 3.

In Fig. 3, the right side of the signal mainly shows background noise such that the zero crossing rate is large. Significant low-frequency signal interference is present on the left side of the signal such that the zero-crossing rate is relatively low. This approach can supplement the performance of short-term energy, and if the detection of traffic flow can combine the short-term energy with short-term zero crossing rate, the endpoint of the signal can be determined more accurately. Therefore, a good result can be obtained by combining the two characteristic parameters of short-term energy and short-time zero crossing rate as vibration characteristic parameters to detect vehicle passage.

## D. VEHICLE SPEED ESTIMATION

The vehicle speed is one of the most important traffic parameters. This study uses multiple data acquisition points to detect vehicle speed. According to the physical definition of the average speed, it is equal to the distance divided by the time. The speed measurement principle is shown in Fig. 4.

Two synchronous vibration signals detect nodes A and B, and the distance is L. When the vehicle passes the two vibration signal detection nodes, we can estimate the speed of the vehicle V according to the detected signal of the time difference between the T and the distance L.

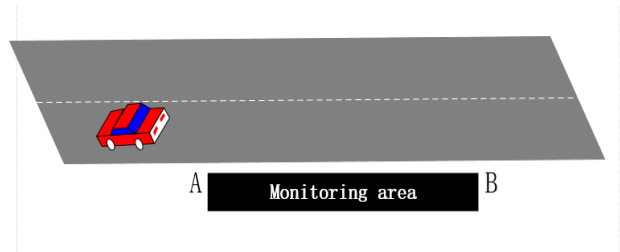


**FIGURE 4.** Speed measurement principle.

When the vibration signal detection node A detects the vehicle entry, the time is recorded as  $t_{A,in}$ , and when the vehicle departs, the time is recorded as  $t_{A,out}$ . In the same way, the detection of vibration signals at node B occur respectively at  $t_{B,in}$  and  $t_{B,out}$ .

The speed estimation formula is written as follows:

$$V = L_{AB}/T \quad (5)$$

$$\Delta t_{in} = t_{B,in} - t_{A,in} \quad (6)$$

$$\Delta t_{out} = t_{B,out} - t_{A,out} \quad (7)$$

$$v_{in} = L/\Delta t_{in} \quad (8)$$

$$v_{out} = L/\Delta t_{out} \quad (9)$$

$$V = (v_{in} + v_{out})/2 \quad (10)$$

where  $L_{AB}$  is the distance between the starting position of the vibration signal and the end position of the vibration signal (i.e., the distance between A and B), T is the time indicating the start position of the vibration signal A to the end position of the vibration signal (i.e., the time elapsed from A to B), and V is the average speed of the vehicle through the detection area.

$t_{A,in}$  is the time at which the point A can detect the vibration signal,  $t_{A,out}$  is the time at which the point A vibration signal disappears,  $t_{B,in}$  is the time at which the point A can detect the vibration signal,  $t_{B,out}$  is the time at which the point A vibration signal disappears,  $\Delta t_{in}$  is the time difference between the vibration signal detected at point A and point B,  $\Delta t_{out}$  is the time difference between point A and point B when the vibration signal disappears,  $v_{in}$  is the vehicle speed estimation at the beginning of the vibration signal, and  $v_{out}$  is the vehicle speed estimation when the vibration signal disappears.

This study is divided into two portions: vehicle detection and vehicle speed estimation. The DAS technology detects vehicle vibration data, which supplies the basis for subsequent signal processing and analysis. The workflow of traffic flow detection for vehicle vibration data is shown in Fig. 5.

### III. IMPROVED WAVELET THRESHOLD IN VIBRATION SIGNAL

#### A. IMPROVEMENT OF WAVELET THRESHOLD FUNCTION

In wavelet threshold denoising, threshold selection is highly important. If the threshold is too large, the useful signal is filtered out. If the threshold is too small, all of the

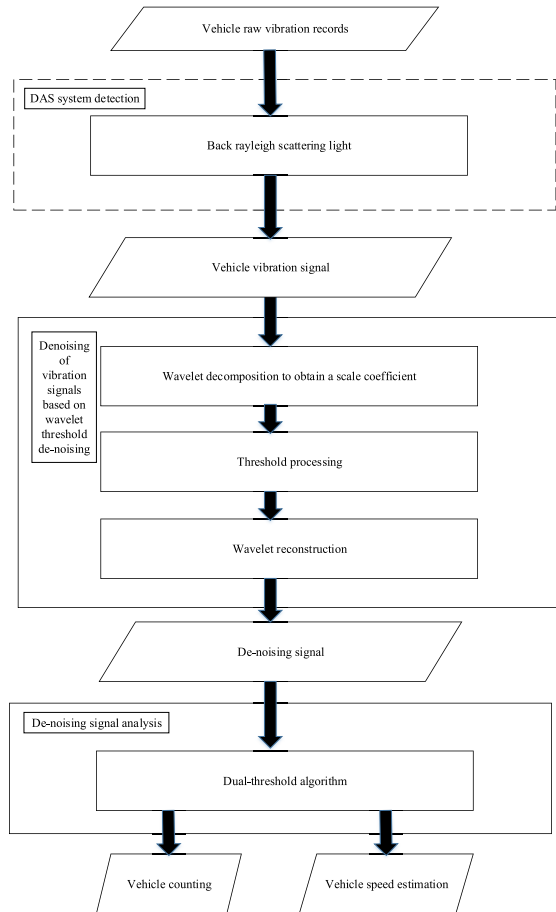


**FIGURE 5.** Summary of the complete workflow.

interference filters cannot be removed. Therefore, the quantization of thresholds directly determines the final noise reduction effect. The traditional threshold function has a hard threshold function and a soft threshold function.

(1) Hard threshold denoising sets the wavelet coefficients with absolute values less than the threshold value to 0 and retains the wavelet coefficients with absolute values greater than the threshold value, and the formula is as written as follows:

$$\overline{\omega_{j,k}} = \begin{cases} 0, & |\omega_{j,k}| < \lambda \\ \omega_{j,k}, & |\omega_{j,k}| \geq \lambda \end{cases} \quad (11)$$

where  $\overline{\omega_{j,k}}$  are the estimated wavelet coefficients, and  $\lambda$  is a given threshold.

It is known from the above formula that hard threshold denoising is not continuous near the threshold point. In the process of denoising, the shock of the reconstructed signal occurs, which produces a larger variance.

(2) Soft threshold denoising sets the wavelet coefficients with absolute value less than the threshold value to 0 and the wavelet coefficients with absolute values greater than the threshold value to minus a constant, and the formula is written

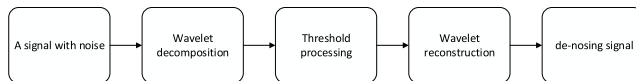


**FIGURE 6.** Flow chart of wavelet threshold denoising step.

as follows:

$$\bar{\omega}_{j,k} = \begin{cases} 0, & |\omega_{j,k}| < \lambda \\ \text{sign}(\omega_{j,k})|\omega_{j,k} - \lambda|, & |\omega_{j,k}| \geq \lambda \end{cases} \quad (12)$$

where sign represents the symbol for the value.

It is known from the above formula that soft threshold denoising is continuous on the whole, but when  $|\omega_{j,k}| \geq \lambda$ , a constant deviation exists.

Classical soft and hard threshold denoising has achieved good results in practical application and also carries its own advantages and disadvantages. The wavelet coefficients of soft threshold denoising are continuous and smooth. However, for constant compression, the wavelet coefficients are larger than the threshold, and certain useful high-frequency information is lost, which affects the authenticity of reconstructed signals. Hard threshold denoising can avoid the constant deviation of the soft threshold. However, because the wavelet coefficients are not continuous at  $\pm\lambda$ , selected additional oscillations appear in the reconstructed signal and worsen the reconstructed signal's smoothness. Therefore, the use of soft threshold denoising or hard threshold denoising is not ideal for reduction of noise.

To overcome these shortcomings, an improved threshold processing function is proposed in combination with a large number of simulation studies, and the formula is given as follows:

$$\bar{\omega}_{j,k} = \begin{cases} 0, & |\omega_{j,k}| < \lambda \\ \alpha \text{sign}(\omega_{j,k})|\omega_{j,k} - \lambda| + (1 - \alpha)\omega_{j,k}, & |\omega_{j,k}| \geq \lambda \end{cases} \quad (13)$$

where  $\alpha = 1/\exp(\frac{|\omega_{j,k}| - \lambda}{m})$ , and m is a normal number. When  $m \rightarrow 0$ ,  $\alpha \rightarrow 0$ , the improved threshold function  $\bar{\omega}_{j,k}$  becomes a hard threshold function. When  $m \rightarrow \infty$ ,  $\alpha \rightarrow 1$ , the improved threshold function  $\bar{\omega}_{j,k}$  becomes a soft threshold function.

Analysis shows that when  $\omega_{j,k} = \lambda$ ,  $\alpha = 1$ ,  $\bar{\omega}_{j,k} = 0$ , that is, when  $\omega_{j,k} \rightarrow \lambda$ ,  $\alpha \rightarrow 1$ ,  $\bar{\omega}_{j,k} \rightarrow 0$ , the improved threshold function  $\bar{\omega}_{j,k}$  in  $\omega_{j,k} = \lambda$  is continuous, overcomes the shortcomings of the hard threshold function in  $\pm\lambda$  is not continuous, and improves the smoothness of the reconstructed signal. With  $\omega_{j,k}$  and  $\bar{\omega}_{j,k}$  increased, and if  $\omega_{j,k} \rightarrow \infty$ ,  $\alpha \rightarrow 0$ ,  $\bar{\omega}_{j,k} \rightarrow \omega_{j,k}$ , and the improved threshold function  $\bar{\omega}_{j,k}$  to  $\omega_{j,k}$  as the asymptote overcomes the soft threshold function, shortcomings of constant bias exist.

The denoising algorithm based on the improved wavelet threshold can be divided into three specific steps: signal wavelet decomposition, threshold processing of wavelet coefficients, and signal reconstruction after threshold processing. The denoising step is shown in Fig. 6.

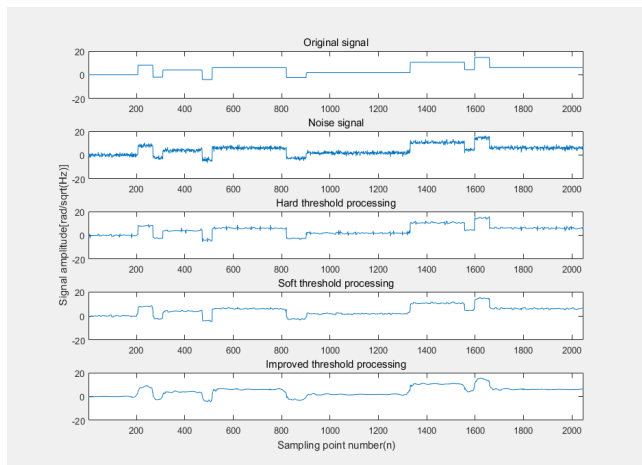


**FIGURE 7.** Signal denoising results of several methods.

## B. SIMULATION EXPERIMENT ON IMPROVED THRESHOLD DE-NOISING

To verify the effectiveness and superiority of the improved threshold function in the denoising algorithm, this section describes the MATLAB simulation software designed to add white noise to the block signal, and the signal is denoised with the hard threshold, soft threshold and improved threshold. The db1 wavelet is used to decompose the noisy signal with 3 layers of the wavelet.

Fig. 7 shows the block signal that uses the hard threshold, soft threshold and improved threshold denoising algorithm to simulate the denoising results. It is clear that hard threshold and soft threshold denoising display varying degrees of waveform distortion, and the improved threshold denoising algorithm achieves a better denoising effect.

To further quantify the denoising results, the denoising algorithm is evaluated using the signal-to-noise ratio (SNR) and the root mean squared error (RMSE). The formulae are written as follows:

$$\text{SNR} = 10 \lg \frac{\sum_n s(n)^2}{\sum_n (s(n) - \hat{s}(n))^2} \quad (14)$$

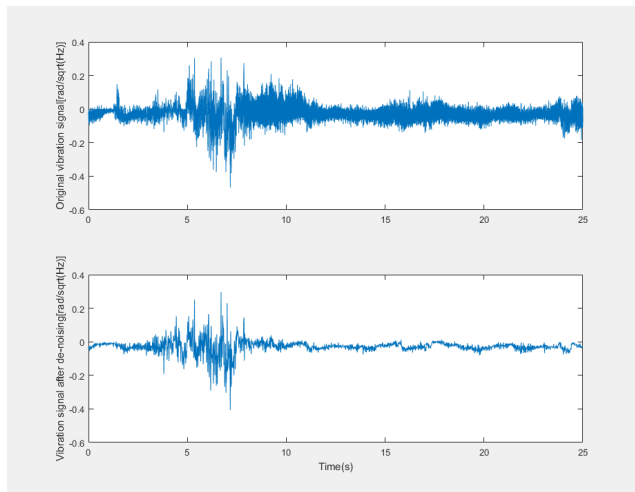
$$\text{RMSE} = \sqrt{\frac{1}{n} \sum_n (s(n) - \hat{s}(n))^2} \quad (15)$$

where  $s(n)$  is the original signal,  $\hat{s}(n)$  is the estimated signal after wavelet threshold denoising, and  $n$  is the sampling point.

Table 1 lists the results of evaluation of the signal-to-noise ratio and the root mean square error of the signal obtained by different threshold denoising methods. According to the data in Table 1, compared with the traditional threshold denoising, the signal-to-noise ratio and the root mean square error of the improved threshold denoising were improved to a certain extent. The denoising signal obtained by the improved threshold denoising method has the best performance parameters. From the analysis in Fig. 7 and Table 1, it can be observed that the improved wavelet threshold denoising signal can

**TABLE 1.** Signal-to-noise ratio and root mean square error of different threshold denoising algorithms.

	Hard threshold	Soft threshold	Improved threshold
Signal-to-noise ratio	5.4594	21.1122	22.3566
Root mean square error	1.0110	0.5274	0.4570

**FIGURE 8.** Original vibration signal and improved wavelet threshold denoising results.

reconstruct the peak value of the signal, and it has smooth features. The improved threshold denoising combined with the traditional wavelet threshold denoising has an advantage, and the filtering effect is better than the traditional wavelet threshold denoising effect.

### C. WAVELET THRESHOLD DE-NOISING OF VEHICLE VIBRATION SIGNAL

The vehicle vibration signal consists of vibration and noise. For a more objective evaluation of the nonstationary vibration characteristics of vehicles, it is necessary to denoise the signal prior to the corresponding analysis of vehicle vibration signals. In this paper, an improved wavelet threshold denoising algorithm is used to reduce the noise of the vehicle vibration signals. First, the original signal is analyzed using five levels of the wavelet, the threshold is selected to filter all of the decomposed signals, and the signal is finally reconstructed. The signal waveform of the original signal and the wavelet threshold denoising are shown in Fig. 8.

As shown in Fig. 8, the peak and abrupt portion of the signal is preserved effectively using wavelet threshold denoising for the vibration signal. Therefore, use of the improved wavelet threshold denoising to analyze the nonstationary vibration signal is effective, and it shows good denoising performance.

## IV. IMPROVED DUAL-THRESHOLD ALGORITHM IN VIBRATION SIGNAL

### A. ENDPOINT DETECTION OF VIBRATION SIGNAL BASED ON IMPROVED DUAL-THRESHOLD ALGORITHM

The dual-threshold algorithm can be used to analyze the vehicle vibration signal. The dual-threshold algorithm is combined with the short-term energy and short-term zero crossing rate to determine from the vibration signal whether a vehicle is passing. When the vehicle passes, the short-term energy function distribution of the vibration signal shows the following characteristics. First, when the vehicle passes through the detection area, the energy-time distribution function of the vehicle signal obtains its maximum value, i.e., an obvious peak value occurs. Second, the energy-time distribution function of the vehicle vibration signal is symmetrical on both sides of the maximum value, i.e., the vehicle signal energy changes from weak to strong and from strong to weak. According to the characteristics of the energy-time distribution function of the vehicle vibration signal, the vehicle detection characteristic parameters are extracted. In the case of a low signal-to-noise ratio, the energy in the vehicle vibration signal is larger than that of the noise signal, and the zero crossing rate is the same.

When the background noise contained in the vibration signal is relatively small, the starting point and the endpoint obtained using the short-term zero crossing rate are more accurate. However, when the signal-to-noise ratio is relatively small and the noise is larger, the error rate of the vibration signal detected by the short-term zero crossing rate becomes larger. When the signal-to-noise ratio is relatively low, if the traditional dual-threshold algorithm is used to detect vibration signals, noise might be treated as the effective vibration signal, resulting in a notably poor result for vibration signal detection. In this section, an improved dual-threshold algorithm is proposed for the problems in traditional dual-threshold detection algorithms. The improved algorithm retains the superiority of the original algorithm and optimizes the key problem of the original algorithm in the strong noise environment with low detection accuracy. The improved algorithm has strong robustness and anti-noise ability. The improved wavelet threshold denoising process is used to improve the signal-to-noise ratio, and the dual-threshold algorithm is used to detect the starting point and endpoint.

Detection of vibration signals using the improved dual-threshold algorithm includes the following steps: data preprocessing, feature extraction, threshold determination, and endpoint detection. The data preprocessing uses the improved wavelet threshold algorithm to denoise the vibration data and improve the signal-to-noise ratio. The feature extraction process converts a series of vibration signal data into characteristic parameters and separates the vibration signal from the background noise area using the characteristic parameters. Therefore, feature extraction is the key step in vibration signal detection, and the feature parameter performance directly

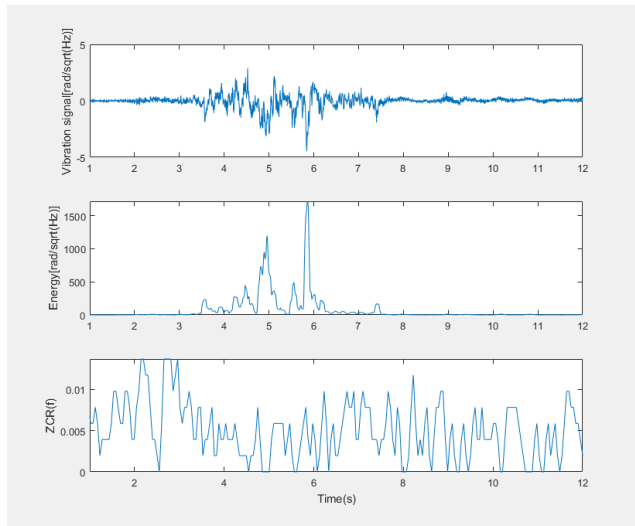


**FIGURE 9.** Traditional dual-threshold algorithm processing results.

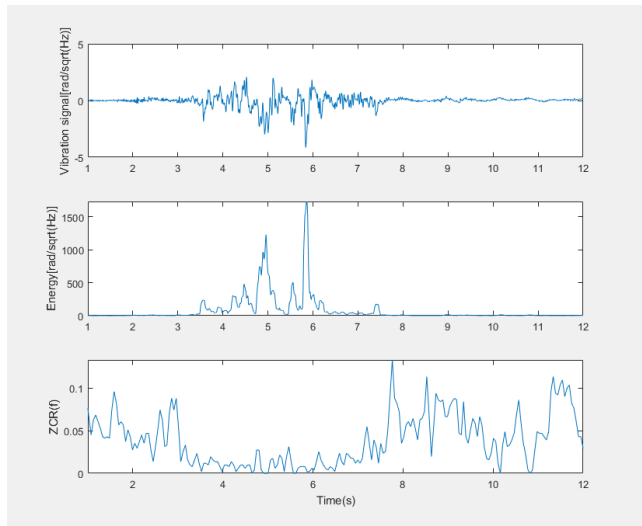
influences the quality of the vibration signal detection and identification rate. The threshold is usually determined by a signal containing only background noise. In general, two thresholds are selected: a high threshold  $T_{\max}$  and a low threshold  $T_{\min}$ , and  $T_{\max} > T_{\min}$ . The  $T_{\min}$  value is relatively small and is generally easily exceeded. The  $T_{\max}$  value is relatively large, and a vibration signal with a certain intensity can pass. The endpoint detection is based on the feature extraction and the determined threshold value. The characteristic parameters of each datum are compared with the thresholds to distinguish the vibration section from the noise section and determine the endpoints of the vibration signal.

To verify the detection effect of the proposed improved dual-threshold algorithm, the traditional dual-threshold algorithm and the improved dual-threshold algorithm are used to process and analyze the typical vehicle vibration signals.

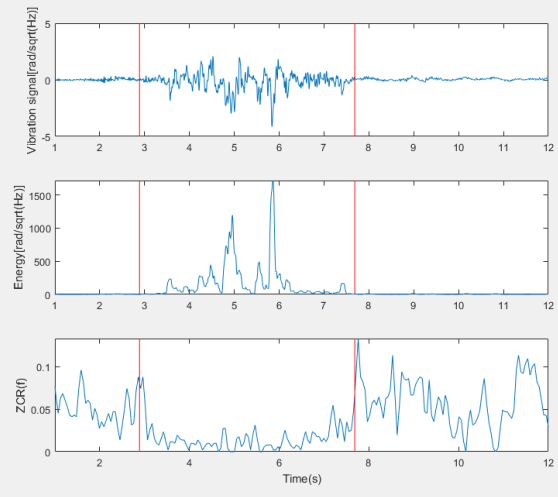
Fig. 9 and Fig. 10 show the short-term energy and short-term zero crossing rates obtained using the traditional dual-threshold algorithm and the improved dual-threshold algorithm, respectively. In the figure, the abscissa is the time domain time axis, and the ordinate is the amplitude of the vibration signal.

From the analysis in Fig. 9 and Fig. 10, the short-term zero crossing rate is close to the vibration signal segment and the no-vibration signal segment when the signal-to-noise ratio is low. This is actually quite easy to understand because the noise is rich in high frequency and high energy, and its zero crossing rate is obviously high. When the signal-to-noise ratio is relatively low, the difference in the noise frequency and the vibration signal frequency is small. Therefore, it is difficult to determine the endpoint vibration signal directly via the short-term zero crossing rate and short-term energy.

Fig. 11 shows the start and end positions of the vibration signal calculated by the vehicle vibration signal using the improved dual-threshold algorithm. The first red line in the



**FIGURE 10.** Improved dual-threshold algorithm processing results.



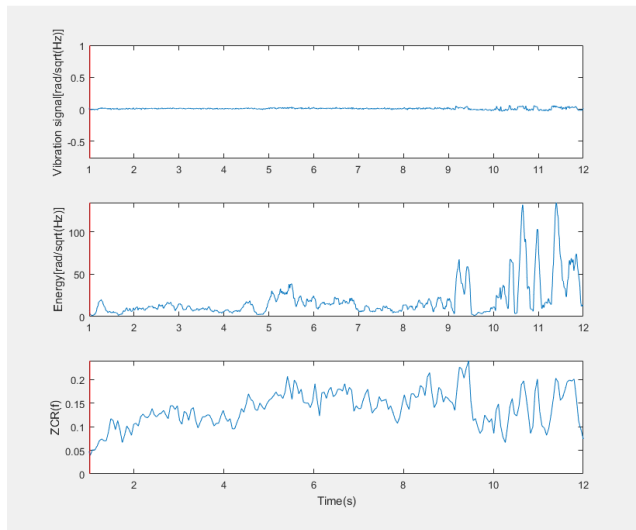
**FIGURE 11.** Improved dual-threshold algorithm for endpoint detection of the vibration signal.

figure is the initial position at which the fiber detects the vibration signal of the vehicle, and the second red line is the end position at which the fiber detects the vibration signal of the vehicle.

Fig. 12 shows the endpoint detection of the vibration signal with only background noise. It is clear that in the absence of vehicle vibration, the short-term energy and the short-term zero crossing rate cannot reach the corresponding threshold, and the detected signal cannot pass through the vehicle.

## V. EXPERIMENTAL FIELD STUDIES

To verify the detection ability of DAS and the processing and analyzing ability of the algorithm proposed in this paper, an experimental study is conducted in the Ma'anshan iron mine. The optical fibers are installed on the side of the road to detect the vibration signals of the vehicles that pass through



**FIGURE 12.** Improved dual-threshold algorithm for endpoint detection of background noise.



**FIGURE 13.** Overhead view of the Nanshan Iron Mine.

the area. This road is chosen as an experimental site because the traffic conditions and the road condition can satisfactorily represent the average condition of the entire field road.

#### A. EXPERIMENTAL SETUP

The data were collected by DAS deployed over an area of approximately 201 m in the NanShan Iron mine (Ma'anshan) as a component of an iron mine seismic trial (see Fig. 14). The optical fiber was located on the road shoulder close to the traffic lane. An overhead view of the Nanshan Iron Mine is shown in Fig. 13.

The main experimental location is the No. 1 monitoring platform of the open-pit iron mine. The data acquisition and transmission of DAS are realized using optical fiber cables. The cables are laid in ravines near the No. 1 monitoring platform and fixed with cement mortar. The length is fixed at 201 m. Fig. 14 shows the No. 1 monitoring platform, and the blue line indicates the ridge line for cable laying.

Due to the limitation of monitoring conditions such as power and terrain, the DAS host is installed in the mine monitoring room located 800 meters away from the monitoring



**FIGURE 14.** No. 1 monitoring platform.

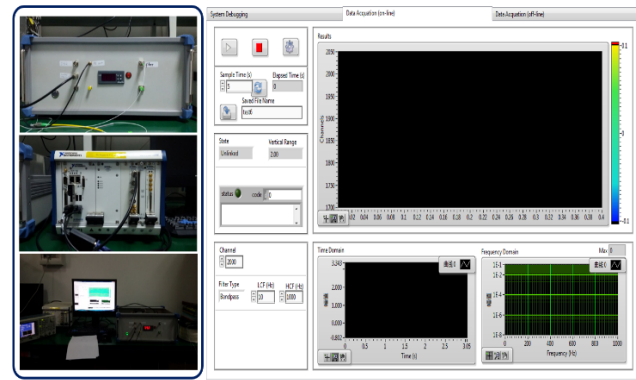


**FIGURE 15.** DAS system.

area. The hardware and software system of the DAS host is shown in Fig. 15 (the left side depicts the hardware system and the right side shows the software system). For optical fiber installation, one end of the fiber is connected to the DAS host, and the other end is bent.

To ensure that the fiber cable is completely coupled with the ground, cement mortar is used to fix the optical fiber cable on the surface of the earth. The length is 102 meters, and other optical fiber cables that are not coupled with the ground are used in data transmission. In data acquisition, only the vibration data in the 201 m optical fiber are collected, including the actual coupling data from the 102 m segment. To ensure the authenticity and reliability of the data, traffic conditions are acquired through on-site video, and vehicle counts and vehicle speeds are obtained when the vehicle passes through the detection area.

For the location of moving vehicles, the recorded data were split into 0.4 ms time intervals (i.e., a collection of 2500 data points per second at each data sampling point).

The seismic signals induced by two types of vehicles were recorded. The two types of manned vehicles were trucks that carry ore and pickups. Trucks that transport ore are divided into two types: full-load vehicles driving up and no-load vehicles driving down.

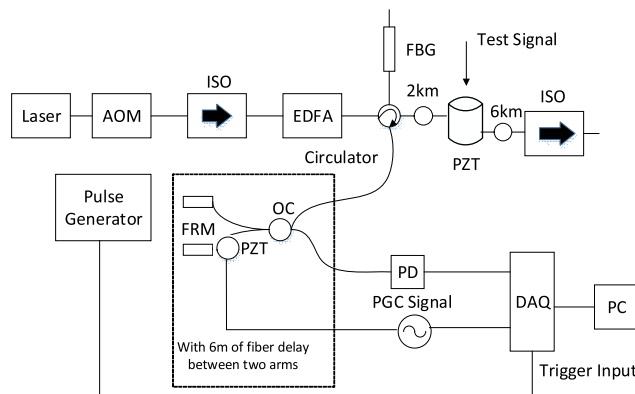


**FIGURE 16.** Setup of the DAS system.

The detection area is composed of 100 sampling points (the interval between the sampling points is 1 meters, and the sampling frequency is 2500 Hz).

This paper analyzed the data collected over a period of 2 days, from 19th May to 20th May 2017.

The setup of the DAS system is illustrated in detail in Fig. 16. The narrow-line-width (3 kHz) laser that produces continuous output at 20 MW and 1550.12 nm is a coherent optical source, and its coherent length is longer than the length of the sensing fiber. The continuous light is modulated by acoustic optical modulator (AOM), and the width and repetition frequency of the pulse are designed and generated by the pulse generator at 30 ns and 10 kHz, respectively. The erbium-doped optical fiber amplifier (EDFA) is used to amplify the pulse light and obtain the appropriate peak power at 1 W and is not affected by the nonlinearity of the sensing fiber. The ASE noise introduced by EDFA is removed by the fiber Bragg grating (FBG) with a 3 dB fiber grating with a narrow bandwidth (0.266 nm, 1550.196 nm central wavelength) and high reflectivity (99%). Pulsed light propagates along the fiber, producing coherent Rayleigh backscattered light. The EDFA, FBG, sensing optical fiber and the Michelson interferometer (MI) are controlled by a four-cylinder circulator. A 6 m fiber imbalance MI and the delay between the two arms are used, and the Rayleigh backscattering light from a particular location affects the output of the MI and the disturbance signal, which is modulated by a sinusoidal PGC signal with a frequency of 1 kHz, and the amplitude is moderated such that the C value is equal to 2.63. The phase of the interference signal carries sensing information such as vibration events. Use of Faraday rotation mirror (FRM) on both arms of the MI can effectively eliminate the influence of polarization fading on the system. A high sensitivity photodetector (PD) with a bandwidth of 50 m was used to monitor the Rayleigh-scattered light trails after coherence. The outputs of the PD and PGC signal are sampled by data acquisition card (DAQ) simultaneously with 200 MS/s sampling rate. The acquired signals on the PD consist of a train of backscattered traces. The length of each track is proportional to the length of the sensing fiber, and the repetition frequency is equal to the pulse

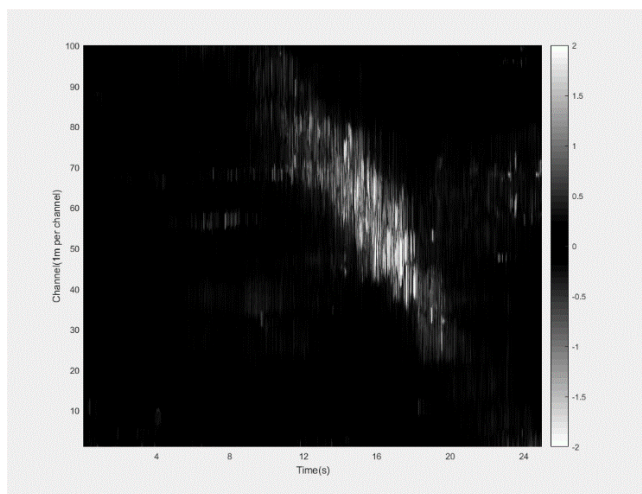


**FIGURE 17.** Vibration signal of a typical vehicle passing through the detection area.

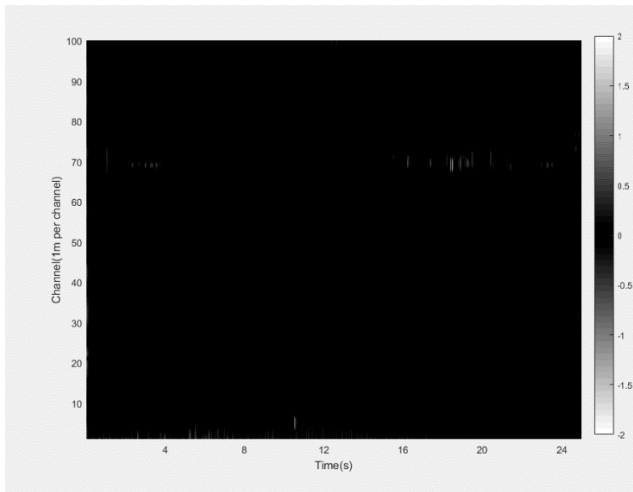
repetition frequency that drives the AOM. Rearranging the trace sequence supplies a callback trace and allows the output from a particular location to be determined as a function of time. The PGC demodulation scheme with arctangent operation is implemented digitally for one particular position along the fiber. A fast Fourier transform is applied to identify the frequency components of any phase perturbation occurring within the gauge length of this point [17].

## B. EXPERIMENTAL RESULTS AND DISCUSSION

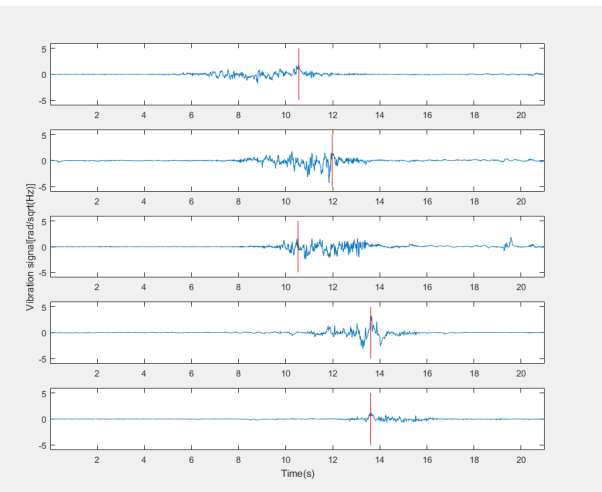
Fig. 17 shows a three-dimensional waterfall figure of a vehicle passing through the detection area. During the production period at Nanshan Mine, the vibration signal was obtained at 15:30. The abscissa in the figure is the time axis, and the ordinate displays 100 sampling points (each sampling point interval is 1 m, and the detection area covers 100 m of continuous sampling). The color in the figure indicates the vibration amplitude of the vehicle passing the sampling point. From Fig. 17, it is clear that the continuous vibration signal is the direction of the seismic source movement, and a subset of the discontinuous vibration signals consists of noise generated by the external factors or the detection devices themselves. It can be observed from the video data that the continuous vibration signal comes from the speed of the pickup vehicle at 20 km/h.

Fig. 18 shows a three-dimensional waterfall figure with background noise. No vehicle passes through the detection area. During the nonproduction period at the Nanshan Mine, the vibration signal was obtained at 19:00. It can be observed from Fig. 18 that if no vehicle passes the detection area during the nonproduction period, only selected noises are present and no continuous vibration signals are observed.

The data shown in Figs. 19, 20, and 21 are the vibration data from a pickup passing through the detection area at 10 km/h. The three figures use the same set of data processed in different ways. Fig. 18 contains five subgraphs showing data collected from five collection nodes at the same



**FIGURE 18.** Vibration signal of background noise.



**FIGURE 20.** Amplitude maximum detection result in the vibration signal.

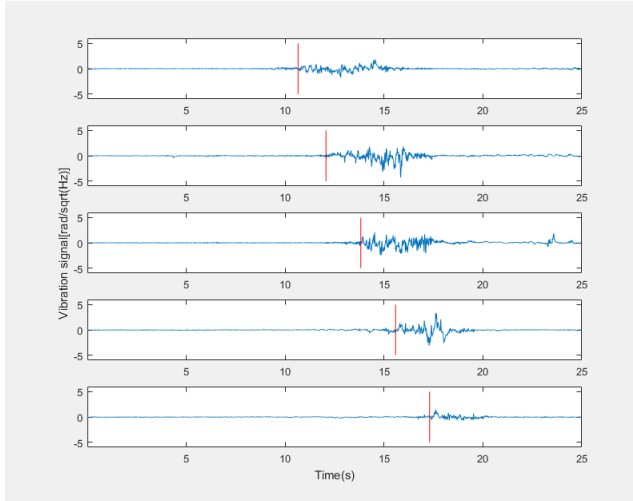


**FIGURE 19.** Improved dual-threshold algorithm for endpoint detection results in vibration signals.

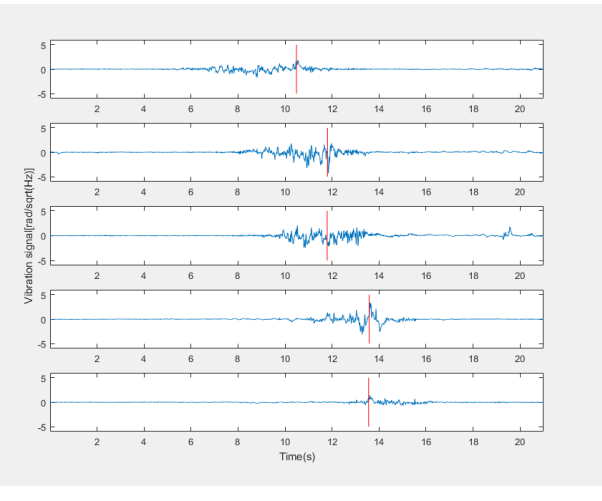


**FIGURE 21.** Energy maximum detection result in the vibration signal.

time. Each data acquisition node is located 5 meters apart. This approach uses the improved dual-threshold algorithm to detect the endpoint of the vibration signal and uses the signal offset among the detection points to detect the vehicle speed. In the subgraph, the red line position is the starting position of the vibration signal.

Fig. 20 shows the detection result of the maximum vibration amplitude. The red line position is the maximum amplitude of the vibration signal at the detection point.

Fig. 21 shows the detection result of the maximum vibration energy. The red line position is the maximum energy value of the vibration signal at the detection point.

It is clear that by improving the dual-threshold method, the time of the vehicle entry into the detection area can be calculated, and the average speed of the vehicle can be calculated using the time elapsed to pass through the detection point. The use of the maximum magnitude signal of the vibration

**TABLE 2.** Vehicle count results.

Time	Actual vehicle flow	Computer statistic results	Error percent
14:30-15:00	17	15	11%
15:30-16:00	19	16	15%

signal to find the offset method is used to detect that the vehicle speed error is large, and the maximum amplitude of some detection points is not generated by the closest distance between the vehicle and the detection point. It is not feasible to use the energy maximum offset of the vibration signal to detect the speed of the vehicle. The peak of the energy peak at each detection point does not change regularly.

The improved dual-threshold algorithm is used to count the vehicles in the detection area, and the results are shown in Table 2.

Comparing the vehicle counts obtained by the improved dual-threshold algorithm with the video recording results,

**TABLE 3.** Speed estimation results (vehicle model: pickup).

Actual vehicle speed (km/h)	20	30	40
Estimated speed (km/h)	19.24	31.36	37.69
Error (%)	-3.8	4.53	-5.77

the improved dual-threshold algorithm can effectively detect whether a vibration source enters the monitoring area. However, the percentage error of detection is still quite large. The reason for this result is that when multiple vehicles continuously pass the detection area, the detection method cannot effectively distinguish the vehicle numbers.

In this paper, a vehicle speed estimation test is designed. In the Nanshan Mine vibration signal detection area, the test vehicle moves at a constant speed, and the vehicle speed is estimated according to the proposed algorithm and compared with the actual speed of the vehicle. In the experiment, the pickup trucks were tested at speeds of 20 km/h, 30 km/h and 40 km/h, each of which was repeated 10 times. The statistical results of each calculation are shown in Table 3. Table 3 shows the comparison between the actual speed and the estimated speed, where the estimated speed is the average of the results of 10 experiments. The experimental results show that this method has good accuracy for vehicle speed estimation, and the range of error can be controlled to less than 6%.

## VI. CONCLUSION

This paper proposes a novel method for traffic flow detection using DAS. To verify the feasibility and effectiveness of the method, a traffic vibration data detection experiment was conducted in Nanshan Mine (Ma'anshan, China). The traffic vibration data were processed and analyzed with the algorithm proposed in this paper. The results show that DAS can effectively detect the traffic vibration signal. For vehicle speed detection, the proposed algorithm can effectively analyze the speed of the moving target. For vehicle counting detection, the algorithm can effectively count single vehicles passing through the detection area, but the vehicle count error is larger when multiple vehicles pass through the detection area. This method of detection offers many advantages over the conventional method because vibration propagation is less sensitive to atmospheric conditions such as wind, moisture, and temperature. DAS supplies non-line-of-sight detection capabilities for a wide range of vehicles and a good detection range and improves detection capability.

In the future, we plan to continue work on traffic flow detection and perform extensive experiments on urban streets and highways with multiple lanes and higher volumes. This study also contains certain drawbacks, and the following difficult problems remain unsolved: (1) Distinguishing the number of vehicles from vibration signals when multiple vehicles pass through the detection area; (2) distinguishing the type of vehicle from the vibration signal; (3) expansion

of the error in data when the detection area increases. It is particularly critical to find a more suitable method to process the data.

## REFERENCES

- [1] F. Qu, F.-Y. Wang, and L. Yang, "Intelligent transportation spaces: Vehicles, traffic, communications, and beyond," *IEEE Commun. Mag.*, vol. 48, no. 11, pp. 136–142, Nov. 2010.
- [2] B. Tian *et al.*, "Hierarchical and networked vehicle surveillance in ITS: A survey," *IEEE Trans. Intell. Transp. Syst.*, vol. 18, no. 1, pp. 25–48, Jan. 2017.
- [3] J. Zhou, D. Gao, and D. Zhang, "Moving vehicle detection for automatic traffic monitoring," *IEEE Trans. Veh. Technol.*, vol. 56, no. 1, pp. 51–59, Jan. 2007.
- [4] C. Zhang, H. Dong, L. Jia, Y. Qin, and Z. Yang, "Robust vehicle detection and identification with single magnetic sensor," in *Proc. IEEE Int. Conf. Intell. Transp. Eng.*, Sep. 2017, pp. 94–98.
- [5] S. J. Park, T. Y. Kim, S. M. Kang, and K. H. Koo, "A novel signal processing technique for vehicle detection radar," in *IEEE MTT-S Int. Microw. Symp. Dig.*, vol. 1, Jun. 2003, pp. 607–610.
- [6] I. Engineering, *Vehicle Detection and Classification Using Wireless Sensor Network*, Tech. Rep., no. 1, 2013, pp. 4845–4856.
- [7] A. Jazayeri, H. Cai, J. Y. Zheng, and M. Tuceryan, "Vehicle detection and tracking in car video based on motion model," *IEEE Trans. Intell. Transp. Syst.*, vol. 12, no. 2, pp. 583–595, Jun. 2011.
- [8] Q. Wang, J. Zheng, H. Xu, B. Xu, and R. Chen, "Roadside magnetic sensor system for vehicle detection in urban environments," *IEEE Trans. Intell. Transp. Syst.*, vol. 19, no. 5, pp. 1365–1374, May 2018.
- [9] S.-L. Jeng, W.-H. Chieng, and H.-P. Lu, "Estimating speed using a side-looking single-radar vehicle detector," *IEEE Trans. Intell. Transp. Syst.*, vol. 15, no. 2, pp. 607–614, Apr. 2014.
- [10] A. Aljaafreh and A. A. Assaf, "A wireless sensor network design and implementation for vehicle detection, classification, and tracking," *Proc. SPIE*, vol. 8713, pp. 34–37, Jun. 2013.
- [11] T. Parker, S. Shatalin, and M. Farhadroushan, "Distributed acoustic sensing—A new tool for seismic applications," *First Break*, vol. 32, no. 2, pp. 61–69, 2014.
- [12] N. Riahi and P. Gerstoft, "The seismic traffic footprint: Tracking trains, aircraft, and cars seismically," *Geophys. Res. Lett.*, vol. 42, no. 8, pp. 2674–2681, 2015.
- [13] E. Martin *et al.*, "Interferometry of a roadside DAS array in fairbanks, AK," in *Proc. SEG Tech. Program Expanded*, 2016, pp. 2725–2729.
- [14] M. F. Duarte and Y. H. Hu, "Vehicle classification in distributed sensor networks," *J. Parallel Distrib. Comput.*, vol. 64, no. 7, pp. 826–838, 2004.
- [15] Y. Kopsinis and S. McLaughlin, "Development of EMD-based denoising methods inspired by wavelet thresholding," *IEEE Trans. Signal Process.*, vol. 57, no. 4, pp. 1351–1362, Apr. 2009.
- [16] S. Kumar, S. Phadikar, and K. Majumder, "Modified segmentation algorithm based on short term energy & zero crossing rate for maithili speech signal," in *Proc. Int. Conf. Accessibility Digit. World.*, Dec. 2016, pp. 169–172.
- [17] G. Fang, T. Xu, S. Feng, and F. Li, "Phase-sensitive optical time domain reflectometer based on phase-generated carrier algorithm," *J. Lightw. Technol.*, vol. 33, no. 13, pp. 2811–2816, Jul. 1, 2015.



**HUIYONG LIU** was born in Yongcheng, Henan, China, in 1986. He is currently pursuing the Ph.D. degree in control science and engineering at Beijing Jiaotong University, Beijing, China. His research interests include intelligent transportation and traffic data analysis and mining.



**JIHUI MA** was born in Jianchang, Liaoning, China, in 1972. He received the B.S. degree in mechanical engineering from the Hangzhou Dianzi College, Hangzhou, China, in 1994, and the M.S. and Ph.D. degrees in transportation system engineering from Beijing Jiaotong University, Beijing, China, in 2008.

From 2005 to 2010, he was an Assistant Professor with the Traffic and Transportation School, where he became an Associate Professor in 2011 and then a Professor in 2017.

He is the author of three books, over 50 articles, and over 10 inventions. His research interests include traffic flow prediction and perception and application of new technology in traffic.



**WENSHENG LIU** was born in Qingcao, Tongcheng, Anhui, China, in 1969. He received the B.S. degree in mining engineering from Chongqing University, China, in 1992, and the M.S. degree in mining engineering from the University of Science and Technology Beijing, China, in 2009, where he is currently pursuing the Ph.D. degree. He is the author of six articles and 15 inventions.



**WENFA YAN** was born in Lulong, Hebei, China, in 1970. He received the B.S. degree in mining engineering from Chongqing University, China, in 1992.

From 2005 to 2010, he was a Field Engineer with the Institute of Mine Seismology, in China and Australia, respectively. From 2013 to 2016, he was an On-Site Project Manager with the Engineering Seismology Group, in China and Canada, respectively.

He is the author of 11 articles, three inventions, and has written over 30 microseism related technical reports. His research interests include rock mechanics and microseismic monitoring technology and its application in traffic, mining, and oil field.



**XI ZHANG** was born in Daming, Hebei, China, in 1953. He received the B.E. degree from Northern Jiaotong University, Shanghai, China, in 1977, the M.E. degree from Kyoto University, Kyoto, Japan, in 1983, and the Ph.D. degree from Beijing Jiaotong University, Beijing, China, in 2004.

He is currently a Professor with Beijing Jiaotong University. His current research interests include intelligent transportation and automation system engineering.



**CONGCONG LI** received the M.S. degree in traffic engineering from Beijing Jiaotong University, Beijing, China, in 2014, where she is currently pursuing the Ph.D. degree with the Department of Traffic and Transportation.

Her research interests include information security and applications in vehicular sensor networks.

• • •